Nano-titania assisted photoreduction of Cr(VI)
The role of the different TiO_2 polymorphs

G. Cappelletti *, C.L. Bianchi, S. Ardizzone

Department of Physical Chemistry and Electrochemistry, University of Milan, Via Golgi 19, 20133 Milan, Italy

Abstract

Nanocrystalline TiO_2 samples, with controlled phase composition, were obtained by combining reactions in solution with mild hydrothermal or thermal treatments. By using as the starting salt $TiCl_3$, pure phase rutile with crystallite sizes of 6 nm and a BET surface area of $130 \, m^2 \, g^{-1}$ was obtained. The photocatalytic activity of the synthesized samples along with that of several commercially available TiO_2 samples, was tested for the photoreduction of Cr(VI). The reaction was performed in TiO_2 aqueous slurry in the presence of different sacrificial molecules (formic acid (FA), isopropyl alcohol (IPA) and sodium sulphite (SS)). The pH of the reaction (2.5) was defined on the grounds of the energy level of the TiO_2 conduction band and of the reduction potential of the Cr(VI)/Cr(III) couple. The reaction kinetics could be described, for all samples, by a pseudo-first order rate equation.

The photocatalytic activity of the anatase–brookite synthesized composite and of the anatase–rutile commercial P25 were found to be the highest (94% at 90 min reaction time). Rutile samples, both synthesized ($\langle d \rangle$ = 6 nm) and commercial ($\langle d \rangle$ = 93 nm), showed a lower activity with respect to the other samples (around 80% at 90 min reaction time). This occurrence is discussed also on the grounds of diffuse reflectance spectra.

Cr(0) was observed at the surface of TiO_2 samples by XPS analyses. Since thermodynamic analysis shows that TiO_2 cannot photoreduce Cr(III) to Cr(0), the formation of Cr(0) is attributed to the reducing action of the produced IPA radicals.

The different contributions to the global reaction pathway are critically discussed.

1. Introduction

Titanium dioxide (TiO_2) is, up to now, one of the most attractive and efficient semiconductor materials suitable for the photodegradation of a variety of organic, biological and inorganic substrates which can be either photooxidized or photoreduced in UV irradiated TiO_2 aqueous suspensions. These processes are based on reactive electrons and holes generated at the surface of the semiconductor when it is illuminated by light with energy larger than its band gap. These electrons and holes may either recombine or become involved in redox reactions [1–14]. Any species, with a reduction potential more positive than that of the conduction band of the semiconductor, can consume electrons, while any species with an oxidation potential more negative than that of the valence band can consume the holes to complete the redox reaction cycle [15].

The photocatalytic activity of titania is deeply influenced by the actual features of the oxide particles, with respect to both structural and morphological characteristics [16]. Structurally TiO_2 can crystallize in three different polymorphs: anatase (tetragonal), rutile (tetragonal) and the metastable brookite (orthorhombic). The photo-activity of anatase is generally considered superior to that of rutile [17]. Anatase is the TiO_2 polymorph stable in the lower temperature domain while rutile forms at temperatures higher than 500–600 °C. The phase transformation to rutile is initiated after the anatase grains have grown to a certain threshold size; in the study by Wang and Ying [18] the critical nuclei size for rutile formation is estimated to be in the range of 40–50 nm. The authors report that once the critical size has been attained rapid rutile formation and grain growth are observed, so that the resulting rutile grains are larger than the

* Corresponding author. Tel.: +39 0250 314219; fax: +39 0250 314300.
E-mail address: giuseppe.cappelletti@unimi.it (G. Cappelletti).

coexisting anatase grains. The direct comparison between the photo-activity of the two polymorphs is, therefore, necessarily affected by unavoidable overlapping effects due to the textural and morphological differences between the two polymorphs. In the light of these effects the first aim of this work was to design reaction paths leading to the formation of pure nanocrystalline anatase and rutile with comparable crystallite sizes and morphology. Further, the synthesis of tailored mixtures of anatase/brookite TiO_2 polymorphs was developed. Coupling of different semiconductors can, in fact, be proposed as a strategy for enhancing the charge separation to reduce charge carrier recombination. In the case of anatase/rutile mixture, the reduced recombination between holes and electrons is considered to be due to the lower energy conduction bands of rutile relative to anatase. Recent reports have also suggested the possibility of electron ''spillover'' from rutile [19]. The activity of the synthesized TiO_2 materials was compared to the one of commercial products with respect to the photoreduction of Cr(VI).

Chromium is widely used in several industrial processes such as metal plating, leather tanning, paint making and others [15,20–25]. Due to its acute toxicity, carcinogenic action and high mobility in water, Cr(VI) is in the list of priority pollutants of most countries. In the 2005 Comprehensive Environmental Responses, Compensation and Liability Act (CERCLA, USA) priority list of hazardous substances, Cr(VI) is at the position 18 (inside the so called Top20, including benzene, arsenic, lead, etc.), while Cr(III) is ''only'' the 218th. In aquatic environments, chromium is present mostly as hexavalent Cr(VI) and trivalent Cr(III). Cr(III) is less noxious and usually immobile through precipitation or adsorption onto solid phase. Therefore the reduction of Cr(VI) to Cr(III) is highly desirable in order to reduce toxicity and contain mobility of chromium ions [21]. After Cr(VI) photoreduction, Cr(III) can be separated from the suspension by several procedures. Lime softening, alum coagulation and iron coagulation have been found capable of removing Cr(III) [15].

A number of studies have been directed to the mechanistic aspects of TiO_2 photoreactions in the case of organic substrates while much less is known about the corresponding interfacial processes involving metal ions. Cr(VI) can be reduced to Cr(III) by TiO_2 since the reduction potential ($E^{\circ}_{Cr(VI)/Cr(III)}$ = 1.33 V, E shifts 138 mV per pH unit) is more positive than that of the conduction band of the oxide. Almost all literature results concerning the photoreduction of Cr(VI) by TiO_2 were performed by adopting as the photocatalyst the well known commercial P25 by Degussa. Only recently TiO_2 and sulphated-TiO_2 powders, prepared by a sol–gel procedure, were employed and the role played by the sulphation treatment in promoting the reduction of Cr(VI) was studied [22].

Further the presence of a hole scavenger is often reported to be needed to promote the reaction [15,20–25], but the actual role played by these molecules either acting as suppressors for electron–hole recombination or directly producing reducing radicals is far from understood.

In this work we report on the activity of nanocrystalline titania samples, prepared in the laboratory with tailored features, with respect to the photoreduction of Cr(VI) in aqueous slurry. The activity of the home-made samples is compared with that of commonly adopted commercial TiO_2 photocatalysts. Different hole scavengers with varying concentrations are employed and the actual role played by the sacrificial molecules is discussed also on the grounds of XPS analyses performed on the used photocatalysts.

2. Experimental

2.1. Sample preparation

All the chemicals were of reagent grade purity and were used without further purification; doubly distilled water passed through a Milli-Q apparatus was used to prepare solutions and suspensions.

Titania samples, except for the well-known P25 Degussa commercial sample (anatase–rutile composite), were named as follows: the letters indicate the polymorphs and the ensuing value the surface area of the samples.

The synthesis of anatase–brookite mixed powder (AB_200) was reported previously by the authors [16,26]. The sol–gel precursor obtained by the hydrolysis of a solution of $Ti(OC_3H_7)_4$ and 2-propanol (water/alkoxide molar ratio = 49 and water/propanol molar ratio = 15) was dried as a xerogel and submitted to a hydrothermal treatment in water (spontaneous pH, $T = 60\,^{\circ}C$, $t = 500$ h). No thermal treatment was performed after the aging.

A similar sol–gel procedure was used to obtained pure anatase crystals (A_215). Few operative conditions were changed: (a) the temperature of hydrolysis was 65 °C, (b) the water/alkoxide molar ratio was 100, (c) a fixed amount of $(NH_4)_2SO_4$ (salt/alkoxide molar ratio = 2) was introduced in the reacting mixture, (d) a washing procedure with a ethanol/water solution (80:20) was introduced in order to remove the salt from the final precursor, (e) a final thermal treatment at 300 °C for 5 h in O_2 stream.

The pure rutile sample (R_130) was obtained starting from a $TiCl_3$ salt solution (12% in hydrochloric acid) by successive addition of two ammonia solutions at different concentrations (2 and 0.5 M), in order to achieve pH 4. The mixture was kept stirred under O_2 stream (10 L/h) till the disappearance of the blue colour of the slurry (about 5 h) due to the oxidation of $Ti(OH)_3$. Further, a fixed amount of KNO_3 was added (KNO_3/$TiCl_3$ molar ratio = 0.5). The final slurry was centrifuged and the wet precursor was dried in oven at 80 °C overnight. Then the precursor was washed with a solution of ethanol/water (80:20) to eliminate the salt and subsequently calcined at 300 °C in the same conditions of the anatase sample.

Both the pure anatase and rutile powders were compared with pure phase commercial samples A_9 (Alfa Aesar) and R_3 (Aldrich), respectively.

2.2. Sample characterization

Room-temperature X-ray powder diffraction (XRPD) patterns were collected between 10° and 80° (2θ range,

$\Delta 2\theta = 0.02°$) with a Siemens D500 diffractometer, using Cu Kα radiation. Rietveld refinement has been performed using the GSAS software suite and its graphical interface EXPGUI [16]. The broadening due to the instrumental contributions was taken into account by means of a calibration performed with a standard Si powder and the one due to strain were not varied in the fitting procedure. The convergence was in any case satisfactory. The backgrounds have been subtracted using a shifted Chebyshev polynomial. The diffraction peak's profile has been fitted with a pseudo-Voigt profile function. Site occupancies and the overall isotropic thermal factors have been varied.

The average diameter of the crystallites, d, was estimated from the most intense reflection (1 0 1) of the TiO$_2$ anatase phase and (1 1 0) of the rutile one, using the Scherrer equation [27].

Specific surface areas were determined by the classical BET procedure using a Coulter SA 3100 apparatus.

Scanning electron microscopy (SEM) photographs are acquired by LEO 1430.

Diffuse reflectance spectra of the powders were measured on UV–vis scanning spectrophotometer (Perkin-Elmer, Lambda 35), which was equipped with a diffuse reflectance accessory. A TiO$_2$ thin film was placed in the sample holder on integrated sphere for the reflectance measurements. A "total white" Perkin-Elmer reference material was used as the reference. The experimental absorption versus lambda plot was elaborated by differentiation to better highlight the different optical features of the catalysts.

X-ray photoelectron spectra were taken in an M-probe apparatus (Surface Science Instruments). The source was monochromatic Al Kα radiation (1486.6 eV). The binding energies (BE) were corrected for specimen charging by referencing the C 1s peak to 284.6 eV, and the background was subtracted using Shirley's method [28]. The fittings were performed using only Gaussian line shapes, without BE or full width at half maximum (FWHM) constraints. The accuracy of the reported BE can be estimated to be ±0.1 eV. With a monochromatic source, an electron flood gun is required to compensate the build up of positive charge on the samples during the analyses, when insulating samples are analyzed: a value of 10 eV has been selected.

2.3. Photocatalytic experiments

Photocatalytic reductions of Na$_2$Cr$_2$O$_7$ (300 μM) were conducted in a Pyrex glass cylindrical reactor with diameter of 120 mm and effective volume of 600 mL. The reactor was thermostated at 25 ± 1 °C during the runs, by continuous water recirculation through an external glass jacket. The system was maintained at pH 2.5; on the grounds of the equilibrium constant $K = [Cr_2O_7^{2-}]/[HCrO_4^-] = 48$, Cr(VI) is mainly speciated as Cr$_2$O$_7^{2-}$ (294 μM). Ionic strength has been kept constant by addition of KNO$_3$ (10^{-2} M). In the photocatalytic experiments three scavengers were used: formic acid (FA), isopropyl alcohol (IPA) and sodium sulphite (SS). The photon source was provided by a 500 W iron halogenide lamp (Jelosil, model HG 500) emitting in the 315–400 nm wavelength range providing a

radiation intensity of I = 2.4 × 10^{-5} einstein dm^{-3} s^{-1}, according to ferrioxalate actinometry [29]. TiO$_2$ nanoparticles (at a concentration of 0.5 g L^{-1}) were sonicated for 15 min in a simple ultrasonic bath before the experiment was started: no damages or structural modification were observed on the TiO$_2$ particles due to this pretreatment. The suspensions were maintained under agitation during the irradiation; aliquots of the reaction solution were withdrawn intermittently. All samples were filtered through a Millipore GSWP 0.22 μm filter before analysis. The concentrations of Cr(VI) were analyzed colorimetrically, using a UV–vis scanning spectrophotometer (Beckman DU 640), adopting the 1,5-diphenylcarbazide method [15].

3. Results and discussion

3.1. TiO$_2$ structural and morphological characterization

3.1.1. Low temperature nanocrystalline anatase and rutile syntheses

In the low temperature domain, where anatase is stable, the third TiO$_2$ polymorph, brookite, can occur, as a metastable phase. The addition of sulphates to the synthetic mixture is commonly reported to depress the formation of brookite and promote the growth of pure anatase. The present, nanocrystalline anatase sample (A_215) was obtained by a sol–gel synthesis performed in the presence of sulphates, followed by a mild thermal treatment at 300 °C. Fig. 1a shows that only the diffraction lines of anatase are appreciable; by elaboration of
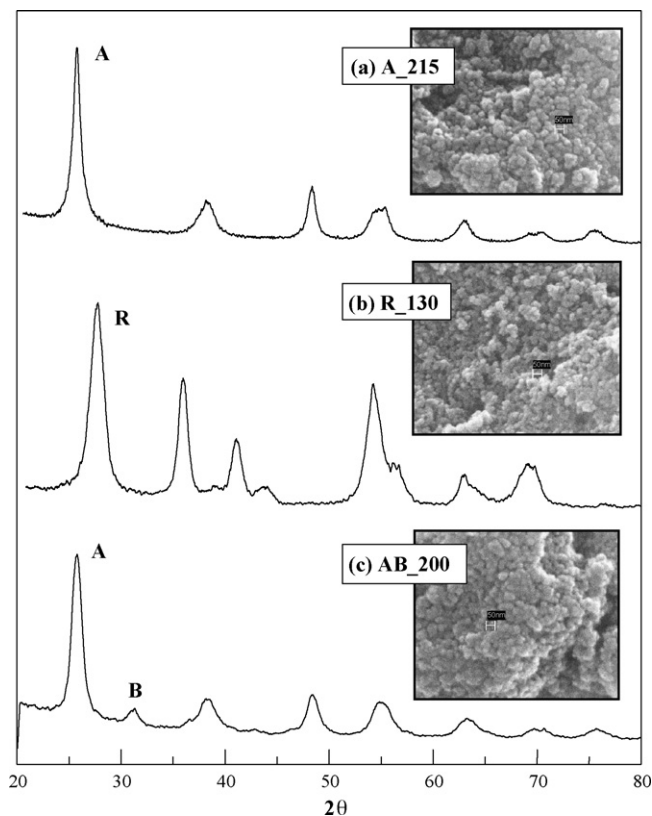
Fig. 1. XRD and SEM images of home-made TiO$_2$ samples. A: anatase, B: brookite and R: rutile.

Table 1
Morphological and structural features of the titania samples, where $\langle d_A^{101} \rangle$ and $\langle d_R^{110} \rangle$ are the relative crystallite sizes obtained by elaborating the 1 0 1 and 1 1 0 most intense peak, respectively

Sample	%A	%B	%R	S_{BET} (m^2 g^{-1})	$\langle d_A^{101} \rangle$ (nm)	$\langle d_R^{110} \rangle$ (nm)
A_215	100	–	–	215 ± 4	7 ± 2	–
A_9	100	–	–	9 ± 1	86 ± 18	–
R_130	–	–	100	130 ± 2	–	6 ± 2
R_3	–	–	100	3 ± 1	–	93 ± 20
AB_200	70	30	–	200 ± 4	7 ± 2	–
P25	80	–	20	50 ± 2	25 ± 5	35 ± 8

the 1 0 1, most intense, peak, the size of 7 nm for the crystallites can be obtained. The SEM micrograph (Fig. 1a) shows the presence of raspberry-like aggregates of variable sizes (30–100 nm). The surface area is consistently rather large (Table 1). Table 1 reports also for the sake of comparison, data of a high purity, commercial anatase sample (A_9).

The synthesis of nanosized rutile is challenging because the traditional methods, either annealing amorphous precursors at elevated temperature or directly flame oxidizing titanium salts inevitably result in large crystallites and irregularly shaped particles. Some authors report reactions performed in micro-emulsions or in reverse microemulsions followed by autoclave growth [30]. These preparations are very complex and a possible organic contamination of the final product cannot be excluded. Other authors report on the role played by specific cations and anions in promoting rutile growth [31,32]. Pedraza and Vazquez [31] used $TiCl_3$ as titanium source and directly oxidized it at room temperature to prepare rutile but anatase also existed in the products. Cheng et al. [32] found that the mineralizer $SnCl_4$ and NaCl reduce markedly the grain size and favour the formation of rutile. The present nanocrystalline rutile synthesis is very simple, but its success relies on the very accurate control of the conditions of each step of the reaction. The reaction implies the precipitation of $Ti(OH)_3$ from solutions of $TiCl_3$ at pH 4, the ensuing oxidation by O_2 at room temperature, the overnight aging in the presence of KNO_3 and the final mild thermal treatment at 300 °C. Fig. 1b shows the diffraction line of the pure rutile sample: no other lines besides those pertaining to the rutile structure are appreciable. The crystallite size is 6 nm, more than one order of magnitude smaller than the high purity commercial rutile, R_3, and an ensuing much larger surface area (Table 1). The SEM micrograph of this sample is also reported in Fig. 1b.

The anatase/brookite composite (AB_200) was obtained by a single sol–gel reaction by modifying the reaction conditions. An intermediate value of water/alkoxide ratio (W/A = 50) together with room temperature conditions and neutral pH were adopted for the hydrolysis and polycondensation reactions. The gels were dried as xerogels and submitted to the mild hydrothermal treatment. Fig. 1c shows the presence of both the anatase and brookite polimorphs. The phase enrichment obtained elaborating the diffractograms by the Rietveld method is 70/30 (Table 1). The crystallite size is 7 nm and that the surface area is, consistently, rather large. The relative crystallite

sizes and surface area for P25 Degussa are also reported in Table 1 for comparison. SEM micrograph is also reported showing aggregates with a regular morphology (Fig. 1c).

3.2. Photocatalytic experiments

3.2.1. Choice of the reaction conditions

The reduction potential of Cr(VI) to Cr(III) is pH dependent and the thermodynamic driving force decreases with increasing pH, the reduction being favoured at low pH (Fig. 2). Consequently pH 2.5 was selected for all the present experiments. O_2 would compete with the photoreduction. Preliminary tests performed either in the absence or in the presence of oxygen, at the adopted pH, showed no appreciable effects on the Cr(VI) reduction. These observations are in agreement with data by Wang et al. [15] who observed that the reaction was not significantly influenced by oxygen at pH 2.5. Opposite results were instead reported by Wei and co-workers [33] at pH 10. Fig. 2 clearly shows that while the thermodynamic driving forces for the reduction of Cr(VI) and O_2 are similar at pH 2.5, at pH 10 the driving force for oxygen is higher and consequently the competition for the photogenerated electrons is larger.

As discussed above, several reasons support the choice of operating at acid pH. However the interfacial electrification features of the oxide and its adsorption behaviour cannot be neglected. The point of zero charge of TiO_2 is, as a rule, around pH 6 and at acid pH the surface charge of the oxide is positive. The depletion from the solution of the anionic chromates (or of dichromates) by adsorption onto the oxide, supported by attractive electrostatic interactions cannot be excluded. Consequently in order to depress, at best, adsorption phenomena all experiments were performed in the presence of a relatively concentrated base electrolyte, which compressing the diffuse double layer, should reduce the attractive potential at the locus of adsorption.
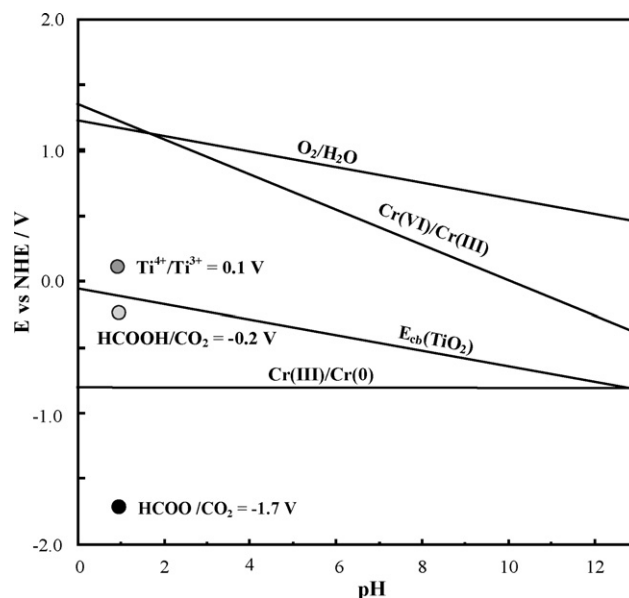

Fig. 2. Energy level of the conduction band of TiO_2 and redox potentials of chromium ions and of relevant species as a function of pH.
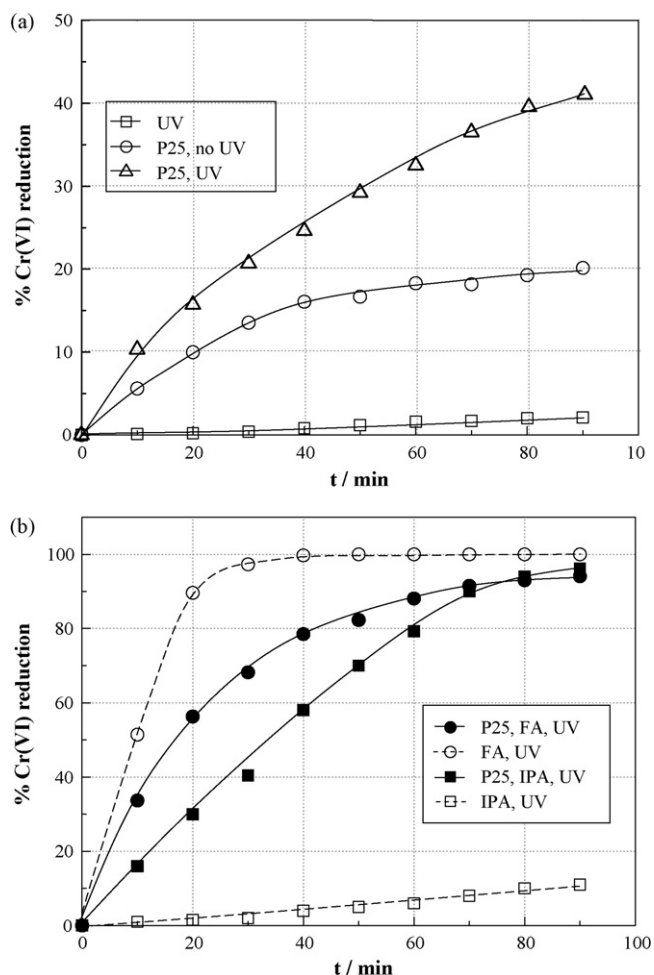
Fig. 3. (a and b) Photocatalytic reduction of Cr(VI) in a slurry system. *Experimental conditions*: [P25] = 0.5 g L^{-1}, [KNO$_3$] = 10^{-2} M, [Cr(VI)]^0 = 300 µM, [scavenger] = 1 M, pH 2.5.

The preliminary part of the work was performed by adopting as photocatalyst the commercial sample, P25 by Degussa. Fig. 3a shows the %Cr(VI) reduction as a function of the reaction time. The direct photolysis of Cr(VI) in the absence of a photocatalyst is negligible. Also negligible is the reduction of Cr(VI) in the dark and in the absence of TiO$_2$, but in the presence of the scavengers. In the absence of irradiation, the depletion by adsorption reaches, a value of around 20% at 90 min reaction time. This adsorbed amount is slightly lower than the value, 24.4%, reported by Wang et al. [15] at pH 2.5 after 60 min reaction time. The reduction performed in the presence of the photocatalyst reaches a value of around 40% at 90 min. The addition of organic additives to promote the photoreduction of Cr(VI) by TiO$_2$ is frequently reported in the literature [19–25]. Formic acid (FA) is one of the more frequently adopted hole scavengers. Isopropyl alcohol (IPA), citric acid [20], humic acids [25] and several organic compounds containing carboxylic groups [21], have been adopted. In the present case FA, IPA and SS were tested as sacrificial molecules. Unfortunately the presence of SO$_3$$^{2-}$ interfered with the analytical determinations of Cr(VI) by the 1,5-diphenylcarbazide method and this scavenger had to be abandoned. Fig. 3b shows that in the

present case, the addition of either FA or IPA definitely promotes the reaction, producing reductions around 94% after 90 min. The figure reports also, for the sake of comparison, the curves relative to the Cr(VI) reduction obtained by irradiating the solution containing the scavenger in the absence of TiO$_2$. In the case of IPA the amount of Cr(VI) reduced at the end of the reaction is around 10%, indicating that the organic radicals produced by direct photolysis of the molecule are not numerous enough to lead to a significant reaction advancement. The case of formic acid is instead very different. The Cr(VI) reduction in the sole presence of irradiated FA (HCOOH) is faster than by the addition of TiO$_2$. This means that formic acid radicals, produced by photolysis, directly reduce Cr(VI) with no support by the photocatalyst. A similar reduction of Ni(II) by photoinduced radicals, such as HCOO$^\bullet$, has been reported in the literature [15]. In the case instead of the reduction of Cr(VI) several authors conclude that formic acid enhances the photoreduction rate by mainly suppressing electron–hole recombination and not by producing radicals [15 and references therein].

The conditions adopted in the diverse experiments reported in the literature may differently affect the reaction path but, in general it can be considered that, the reduction potential of HCOO$^\bullet$/CO$_2$, −1.7 V versus SHE [34], is a very negative value, enough to reduce Cr(VI) and even to reduce Ti(IV) (see Fig. 2). Fig. 4 actually shows XPS spectra of Ti 2p and oxygen 1s obtained, on P25 samples withdrawn from the suspension at the end of the reduction reaction, respectively in the case of IPA and FA as hole scavengers. It can be immediately observed that in the case of IPA the Ti 2p region is regular showing the presence of only one component attributable to Ti(IV) in TiO$_2$ at 458.4 eV. The same can be observed in the case of the oxygen peak, which shows the common two components attributable respectively to reticular oxygen and to surface OH groups [35]. The picture changes significantly when FA is used as a scavenger. The presence of a second component, with a lower BE (457.3 eV) attributable to Ti(III) in oxides [36] is clearly evidenced in the Ti 2p doublet. Also the oxygen peak is in this case broad and shows the presence of a second reticular component which might be attributed to the reduced titanium dioxide. In the light of results in Figs. 3b and 4, it seems meaningless to use a sacrificial molecule which, on one side, is capable to reduce Cr(VI) by itself and, on the other side, it is so active to even reduce the photocatalyst. Consequently FA was abandoned and all the ensuing experiments were performed with IPA.

Fig. 5 shows the Cr(VI) reduction performed in the presence of different IPA concentrations under otherwise constant conditions. The two curves obtained at the higher concentrations (1 and 0.5 M) show little variation between each other while for IPA 0.1 M a definite decrease in the rate of the reaction is observed. All the following results were obtained in the presence of IPA 0.5 M.

3.2.2. Role of the different TiO$_2$ photocatalysts

The different TiO$_2$ photocatalysts, both synthesized in the laboratory and commercial, whose features are reported in Table 1, were tested for the Cr(VI) reduction in the condition
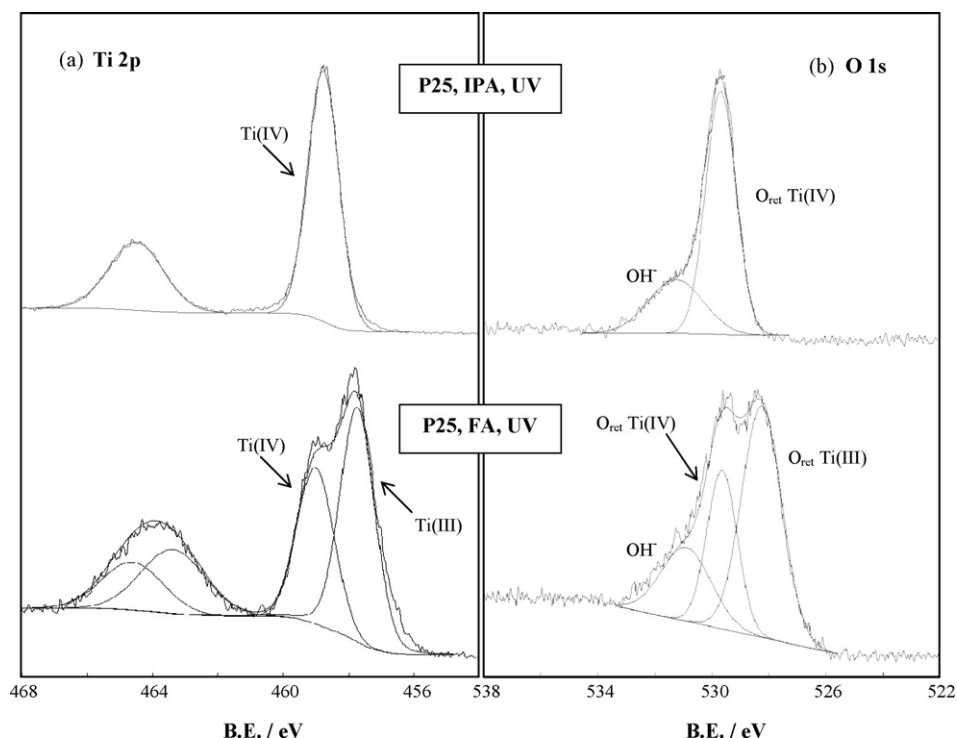
Fig. 4. Fitted spectra of XPS regions: (a) Ti 2p and (b) O 1s in the case of different scavengers for exhausted P25 samples.

reported above, i.e. in the presence of IPA 0.5 M. For all the samples the reaction kinetics can be described by a pseudo-first order rate equation. The rate constant (k) values for the different catalysts, evaluated by linear fitting of the logarithmic plot (Fig. 6), are listed in Table 2 together with the %reduction at 90 min reaction time. The value of the rate constant obtained in the case of the commercial P25 Degussa is fully comparable (mutatis mutandis) with the relative value reported by Wang et al. [15]. The two samples showing the largest k values are the two mixed phase catalysts, AB_200 and P25. Sample A_215, the pure anatase oxide prepared in the laboratory, presents a peculiar behaviour which reflects the sigmoidal shape of the
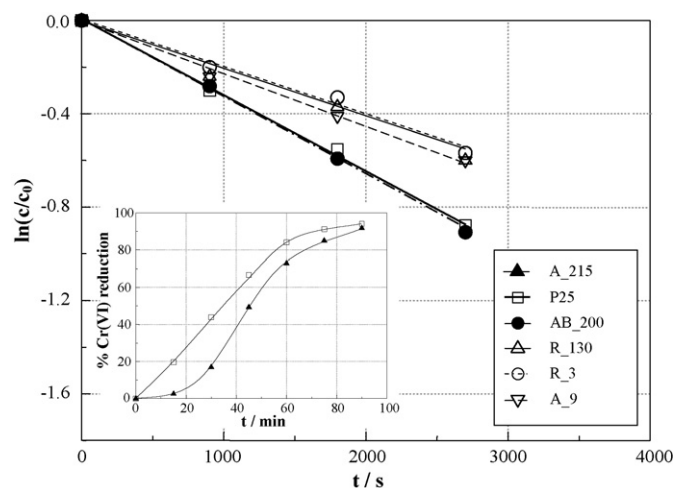

Fig. 6. Logarithmic plot adopted to obtain the rate constant by a simplified first-order rate equation for all the present samples. *Experimental conditions*: $[TiO_2]$ = 0.5 g L^{-1}, $[KNO_3]$ = 10^{-2} M, $[Cr(VI)]^0$ = 300 μM, [scavenger] = 0.5 M, pH 2.5. Inset: photocatalytic reduction of Cr(VI) in a slurry system by selected samples.

Table 2
Photocatalytic kinetic constant and %reduction of Cr(VI) for all samples, in the presence of IPA 0.5 M

Sample	$\kappa \times 10^4$ (s^{-1})	%Conversion (90 min)
A_215	n.d.[a]	92
A_9	2.3 ± 0.1	84
R_130	2.0 ± 0.1	80
R_3	1.9 ± 0.1	83
AB_200	3.1 ± 0.2	94
P25	3.0 ± 0.1	94

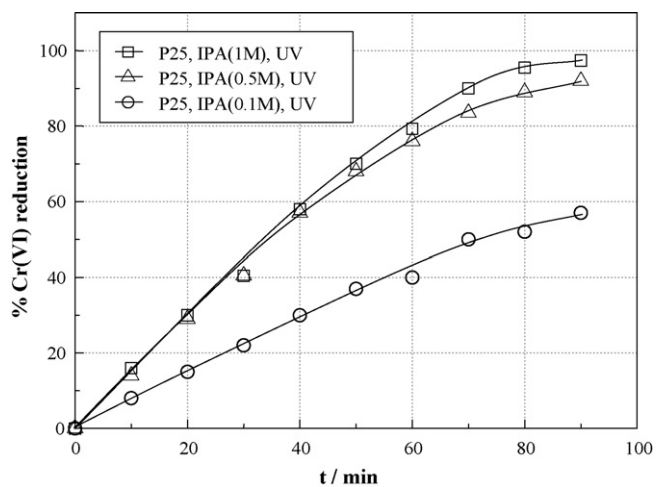[a] Not determined due to the sigmoidal shape of the reduction curve (see inset Fig. 6).

Fig. 5. Photocatalytic reduction of Cr(VI) in a slurry system with different concentrations of IPA scavenger. *Experimental conditions*: [P25] = 0.5 g L^{-1}, $[KNO_3]$ = 10^{-2} M, $[Cr(VI)]^0$ = 300 μM, pH 2.5.

reduction curve (inset Fig. 6). The reduction at short reaction time is poor while after about 30 min the rate increases leading to a reduction at 90 min comparable with the one of the best samples. Due to the shape of the reduction curve, the rate constant, mainly based on short time data, was not evaluated. Besides the particular behaviour of sample A_215 at short reaction times, Table 2 shows that the commercial anatase sample (A_9), presenting a much lower surface area and larger crystallites than A_215, presents a lower global final conversion. This observation indicates that the present reaction is favoured, in the case of the anatase polymorph, by small crystallites and large surface area. This conclusion is not trivial since opposite results are present in the literature concerning the role played by the crystallite size on the performance of TiO$_2$ in photocatalytic reactions [16]. The samples showing the lowest performance are the pure rutile samples, both in the case of the small and of the large crystallite oxides. Data in Table 1 indicate clearly that the rutile polymorph is less favoured than the other TiO$_2$ phases. This result is very interesting since, in the present case, a direct comparison can be made, between anatase (A_215) and rutile (R_130) samples showing the same crystallite sizes. In order to obtain further information concerning the features of the various catalysts, the light absorption behaviour was investigated.

Fig. 7 reports the derivative plots of diffuse reflectance spectra (an example of the experimental plot is reported as an inset) for the present samples. It can be immediately observed in the figure that both anatase and mixed phase samples show a
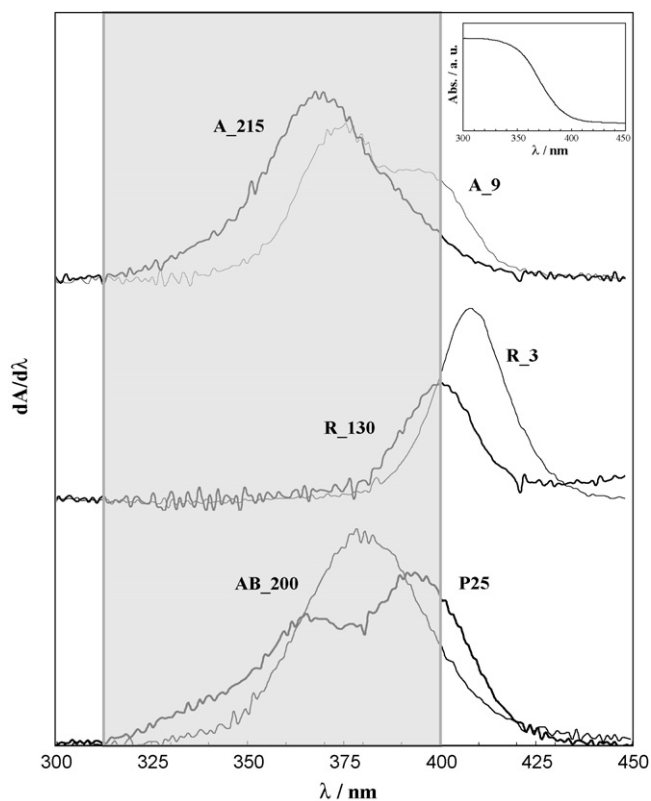

Fig. 7. Derivative plots of diffuse reflectance spectra for all the samples. The grey zone represents the emission wavelength range of the irradiation source. Inset: an example of the experimental plot.

broad absorption region centred in the emitting wavelength of the lamp. The two rutile samples, although characterized by largely different crystallite sizes, show a very similar absorption region shifted in the visible wavelength direction with respect to the other samples. The absorption data show that the rutile polymorphs are not favoured by irradiation in the UV region. It may be stressed that the final Cr(VI) reduction by sample R_130 is about 15% lower than that of sample A_215 although the size of the crystallites is almost the same for the two samples. This difference is therefore to be attributed to intrinsic features of the polymorph (e.g. light absorption, exposed crystalline faces, surface OH density, etc.) and not to superimposed morphological and textural characteristics.

The general better performance presented by the mixed samples is possibly to be traced back to an increase in charge separation efficiency due to interfacial electron transfer via the junction between the different TiO$_2$ polymorphs.

To identify the speciation of chromium after the photocatalytic tests, the TiO$_2$ powders, simply dried, were submitted to XPS analyses. High resolution scans of Cr 2p$_{3/2}$ peaks are shown in Fig. 8 for three representative samples. In all cases the Cr 2p peak is broad and shows the presence of shoulders and humps. The best fit procedure yields the presence of three components attributable respectively to Cr (VI), Cr(III) and Cr(0) (579.4, 576.5, 574.4 eV, respectively [36]). The presence of Cr(0) was not expected since thermodynamically TiO$_2$ is not capable of reducing Cr(III) to Cr(0) (see Fig. 2). A specific role played by IPA must be invoked. Specific potential values of redox couples relative to IPA could not be found in the literature. Serpone et al. [37] report that IPA radicals, produced by photoirradiation in the presence of TiO$_2$, bear a potential negative enough to reduce Ti(IV) to Ti(III). Henglein et al. [38,39] observed in the reduction of silver ions, the formation of silver clusters supported by organic species, which show a markedly different redox behaviour with respect to regular metal ions. On the ground of the present results, it is not possible to discriminate whether Cr(0) is the result of the reduction of adsorbed Cr(III) or of the adsorption on the surface of TiO$_2$ of Cr(0) formed in solution.

In order to obtain direct indications on the possible occurrence of oxidation reactions by IPA which might support the formation of Cr(0), the region of C 1s, on a representative TiO$_2$ sample withdrawn at the end of the photocatalytic reaction, was analyzed.

Four peaks can be observed (Fig. 9) which can be attributed to: simple, even adventitious, hydrocarbons (lower BE, 284.6 eV), C–OH component (286.2 eV) due to the adsorption of IPA, C=O in ketons and aldehydes (287.5 eV) and, at higher BE (288.3 eV), a component due to the presence of carboxylic acid at the surface of the used samples [40]. The presence of oxidized C=O or COOH species supports the occurrence of a redox reaction between IPA radicals, which are further oxidized, and Cr(III) adsorbed at the surface of TiO$_2$, which is further reduced to Cr(0).

The photocatalytic reduction of Cr(VI) possibly occurs by two parallel pathways: one is the direct pathway where metal ions are reduced by reaction with the conduction band electrons
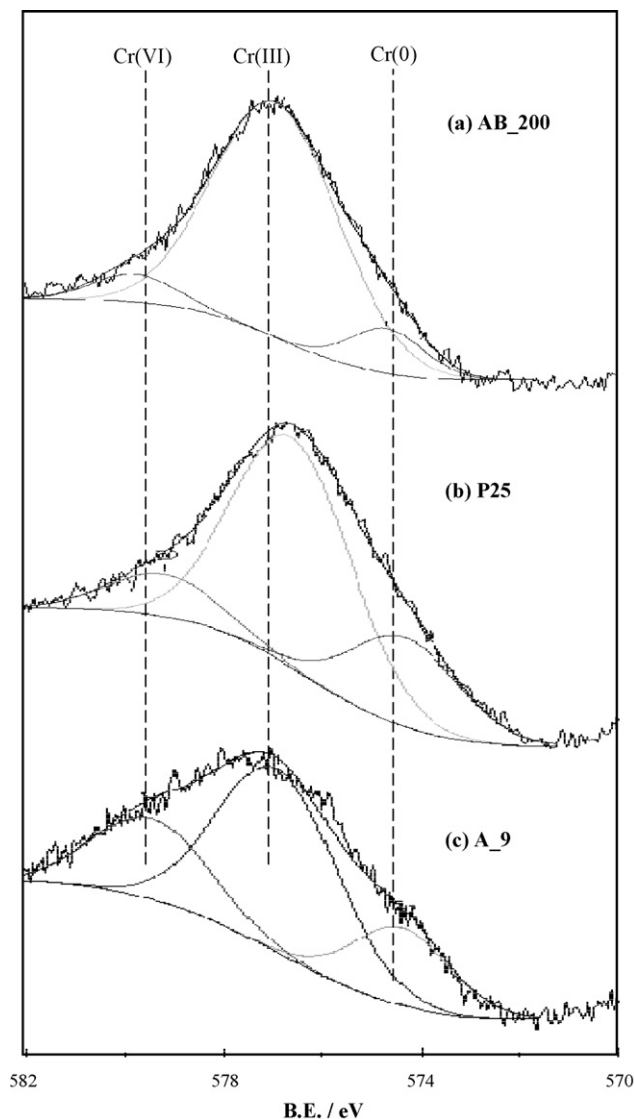
Fig. 8. Fitted spectra of XPS Cr $2p_{3/2}$ region of different samples.
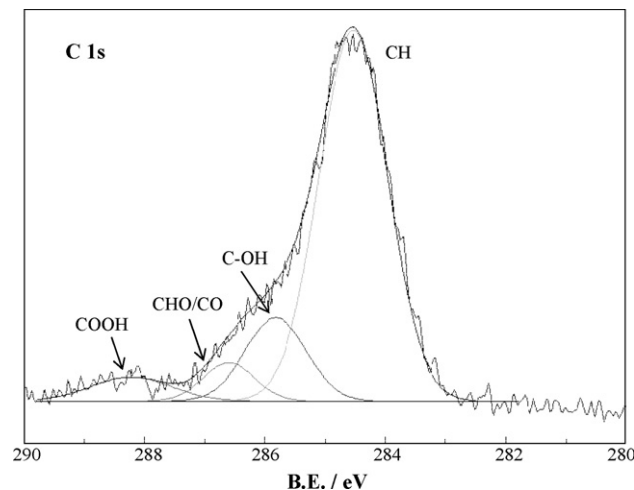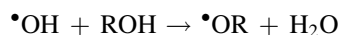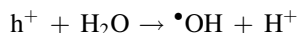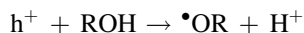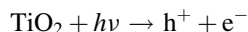

Fig. 9. Fitted spectra of XPS C 1s region of a representative TiO$_2$ sample.

on the TiO$_2$ surface and the other is an indirect pathway where metal ions are reduced by aqueous radical species created by the following steps:

$$TiO_2 + h\nu \rightarrow h^+ + e^-$$

$$h^+ + ROH \rightarrow {}^{\bullet}OR + H^+$$

$$h^+ + H_2O \rightarrow {}^{\bullet}OH + H^+$$

$${}^{\bullet}OH + ROH \rightarrow {}^{\bullet}OR + H_2O$$

In the case instead of the reduction of Cr(III), the only process thermodynamically possible is the reduction supported by radical species produced by the sacrificial molecule.

Energy consumption aspects should be obviously considered when dealing with water purification techniques, but there are few examples in the literature [41]. The energy consumption can be easily calculated taking into account the power of the emitting source and the reaction time. In the present case, for the most active catalysts (AB_200 and P25), the obtained value is 0.75 kWh and the calculation was limited to the energy required to reach a 94% Cr(VI) conversion. This value compares well with parallel literature data and is significantly lower with respect to the photocatalytic degradation of 2-chlorophenol by TiO$_2$ [41].

4. Conclusions

Nanocrystalline TiO$_2$ polymorphs were obtained by combining reactions performed in solution with mild thermal or hydrothermal treatments. Adopting as the starting salt TiCl$_3$ and carefully controlling each step of the reaction, pure phase rutile samples showing crystallite sizes of 6 nm were obtained, in the absence of organic contaminants or of autoclave treatments. This can be considered a significant achievement since the general threshold for rutile formation, by reaction in solution, is 40–50 nm, in mixture with anatase. Pure phase rutile is otherwise formed upon high temperature treatments and in this case crystallites are in the range 80–150 nm. The photocatalytic activity of the synthesized samples along with that of several commercially available TiO$_2$ samples, was tested for the photoreduction of Cr(VI) in the presence of different hole scavengers. The conditions of the reaction were defined on the grounds of the potential/pH relations of the Cr(VI)/Cr(III) couple and of the energy level of the TiO$_2$ conduction band. Of the different hole scavengers, HCOOH showed direct reduction of Cr(VI) even in the absence of TiO$_2$, and provoked the formation of Ti(III) at the surface of the photocatalysts. The direct reduction of Cr(VI) by isopropyl alcohol was, instead, negligible. The reaction kinetics could be described, for all samples by a pseudo-first order rate equation.

The samples showing the best performance were the mixed phase samples, both the anatase–brookite synthesized composite and the anatase–rutile commercial P25, which besides presenting a broad absorption curve at the adopted wavelengths may also present a retarded electrons/hole recombination due to the different polymorph junction. Rutile samples, both synthesized (6 nm) and commercial (93 nm), showed an almost

identical activity which was lower than that of the other samples. It may be stressed that the final Cr(VI) reduction by sample R_130 is about 15% lower than that of sample A_215 although the size of the crystallites is almost the same for the two samples. This difference is therefore to be attributed to intrinsic features of the polymorph (e.g. light absorption, exposed faces, etc.) and not to superimposed morphological and textural aspects. By XPS analyses Cr(0) was observed at the surface of TiO_2 samples at the end of the photocatalytic reaction even if thermodynamic analysis showed that TiO_2 cannot photoreduce Cr(III) to Cr(0). This occurrence is attributed to the reduction of Cr(III), adsorbed at the surface of TiO_2, by the produced IPA radicals. Actually components attributable to carbonyl and carboxylic groups are observed in the XPS C 1s region of TiO_2 suggesting reduction processes directly supported by the sacrificial molecule.

Acknowledgement

References

[1] K. Mogyorosi, A. Farkas, I. Dekany, Environ. Sci. Technol. 36 (2002) 3618–3624.
[2] T. Ozawa, M. Iwasaki, H. Tada, T. Akita, K. Tanaka, S.J. Ito, J. Colloid Interface Sci. 281 (2005) 510–513.
[3] C. Hu, Y.Z. Wang, H.X. Tang, Chemosphere 41 (2000) 1205.
[4] J. Yu, J.C. Yu, M.K.-P. Leung, W. Cheng, B. Ho, X. Zhao, J.J. Zhao, J. Catal. 217 (2003) 69–78.
[5] H. Lin, C.P. Huang, W. Li, C. Ni, S. Ismat Shah, Y.-H. Tseng, Appl. Catal. B: Environ. 68 (2006) 1–11.
[6] S. Bakardjieva, V. Stengl, L. Szatmary, J. Subrt, J. Lukac, N. Murafa, D. Niznansky, K. Cizek, J. Jirkovskyc, N. Petrova, J. Mater. Chem. 16 (2006) 1709–1716.
[7] M. Kolar, H. Mest'ankova, J. Jirkovsky, M. Heyrovsky, J. Subrt, Langmuir 22 (2006) 598–604.
[8] J. Krysa, J. Jirkovsky, J. Appl. Electrochem. 32 (2002) 591–596.
[9] K. Yanagisawa, J. Ovenstone, J. Phys. Chem. B 103 (1999) 7781–7787.
[10] A. Fujishima, T.N. Rao, D.A. Tryk, J. Photochem. Photobiol. C 1 (2000) 1–21.
[11] M. Anpo, T. Shima, S. Kodama, Y. Kubokawa, J. Phys. Chem. 91 (1987) 4305–4310.
[12] A.J. Maira, K.L. Yeung, C.Y. Lee, P.L. Yeu, C.K. Chan, J. Catal. 192 (2000) 185–196.
[13] C.B. Almquist, P. Biswas, J. Catal. 212 (2002) 145–156.
[14] Z. Zhang, C.C. Wang, R. Zakaria, J.Y.M. Ying, J. Phys. Chem. B 102 (1998) 10871–10878.
[15] X. Wang, S.O. Phekonen, A.K. Ray, Ind. Eng. Chem. Res. 43 (2004) 1665–1672.
[16] S. Ardizzone, C.L. Bianchi, G. Cappelletti, S. Gialanella, C. Pirola, V. Ragaini, J. Phys. Chem. C 111 (2007) 13222–13231.
[17] S. Bakardjieva, V. Stengl, L. Szatmary, J. Subrt, J. Lukac, N. Murafa, D. Niznansky, K. Cizek, J. Jirkovskyc, N. Petrova, Mater. Chem. 16 (2006) 1709–1716.
[18] C.-C. Wang, J.Y. Ying, Chem. Mater. 11 (1999) 3113–3120.
[19] D. Hurum, A.A. Agrios, K.A. Gray, T. Rajh, M.C. Thurnauer, J. Phys. Chem. B 107 (2003) 4545–4549.
[20] J.M. Meichtry, M. Brusa, G. Mailhot, M.A. Grela, M.I. Litter, Appl. Catal. B: Environ. 71 (1–2) (2007) 101–107.
[21] S.M. Lee, I.-H. Cho, Y.-Y. Chang, J.-K. Yang, J. Environ. Sci. Health, Part A: Toxic/Hazard. Subst. Environ. Eng. 42 (4) (2007) 543–548.
[22] F. Jiang, Z. Zheng, Z. Xu, S. Zheng, Z. Guo, L. Chen, J. Hazard. Mater. 134 (1–3) (2006) 94–103.
[23] S. Goeringer, C.R. Chenthamarakshan, K. Rajeshwar, Electrochem. Commun. 3 (2004) 290–292.
[24] Y. Ku, I.L. Jung, Water Res. 35 (2001) 135–142.
[25] J.-K. Yang, S.M. Lee, Chemosphere 63 (2006) 1677–1684.
[26] T. Boiadjieva, G. Cappelletti, S. Ardizzone, S. Rondinini, A. Verteva, Phys. Chem. Chem. Phys. 6 (2004) 3535–3539.
[27] C.L. Bianchi, S. Ardizzone, G. Cappelletti, Dekker Encyclopedia of Nanoscience and Nanotechnology, Dekker, New York, 2006 , doi:10.1081/E-ENN-120042107, pp. 1–10.
[28] D. Shirley, Phys. Rev. B5 (1972) 4709.
[29] C.G. Hatchard, C.A. Parker, Proc. R. Soc. Lond. Ser. A235 (1956) 518–536.
[30] M. Andersson, L. Osterlund, S. Ljungstrom, A. Palmqvist, J. Phys. Chem. B 106 (2002) 10674–10679.
[31] F. Pedraza, A. Vazquez, J. Phys. Chem. Solids 60 (1999) 445–448.
[32] H. Cheng, J. Ma, Z. Zhao, L. Qi, Chem. Mater. 7 (1995) 663–671.
[33] W.-Y. Lin, C. Wei, K. Rajeshwar, J. Electrochem. Soc. 140 (1993) 2477–2482.
[34] C.R. Chentamarakshan, K. Rajeshvar, Electrochem. Commun. 2 (2000) 527–530.
[35] G. Cappelletti, C.L. Bianchi, S. Ardizzone, Appl. Surf. Sci. 253 (2006) 519–524.
[36] J.F. Moulder, W.F. Stickle, K.D. Bomben, Handbook of X-ray Photoelectron Spectroscopy, Perkin Elmer, Eden Praire, 1992.
[37] N. Serpone, I. Texier, A.V. Emeline, P. Pichat, H. Hidaka, J. Zhao, J. Photochem. Photobiol. A 136 (2000) 145–155.
[38] A. Henglein, T. Linnert, P. Mulvaney, Ber. Bunsen-Ges. 94 (12) (1990) 1449–1457.
[39] P. Mulvaney, A. Henglein, Chem. Phys. Lett. 168 (3–4) (1990) 391–394.
[40] S. Ardizzone, C.L. Bianchi, G. Cappelletti, Surf. Interface Anal. 38 (2006) 452–457.
[41] V. Ragaini, E. Selli, C.L. Bianchi, C. Pirola, Ultrason. Sonochem. 8 (3) (2001) 251–258.